


Detecting prethermal Floquet phases of Rydberg atom arrays

Somsubhra Ghosh¹, Diptiman Sen², and K. Sengupta¹

¹*School of Physical Sciences, Indian Association for the Cultivation of Science, Kolkata 700032, India*

²*Center for High Energy Physics, Indian Institute of Science, Bengaluru 560012, India*

 (Received 25 April 2023; revised 6 July 2023; accepted 29 August 2023; published 11 September 2023)

We study the prethermal Floquet phases of a two-dimensional Rydberg atom array on a rectangular lattice in the presence of a periodic drive with large drive amplitude. We derive an analytic, albeit perturbative, Floquet Hamiltonian using Floquet perturbation theory (FPT) which charts out these phases and shows that the transition between them can be accessed by tuning the drive frequency. Using both numerical exact diagonalization on finite-size arrays and an analytical first-order Floquet Hamiltonian derived using FPT, we show that these prethermal Floquet phases and the transitions between them can be detected by studying the dynamics of equal-time density-density correlation functions of the Rydberg atoms. Our analysis thus provides a simple way of detecting these phases and associated transitions in this system; such a detection can be achieved in standard experiments, which we discuss.

DOI: [10.1103/PhysRevB.108.094302](https://doi.org/10.1103/PhysRevB.108.094302)

I. INTRODUCTION

Quantum systems involving ultracold atoms in optical lattices have been the subject of intense theoretical and experimental studies in recent years [1–8]. The reason for such interest in these systems stems from their ability to act as emulators of strongly correlated models. Moreover, they allow us to explore parameter regimes and quantum dynamics of the emulated models, which is usually impossible to access in standard laboratory setups. A typical example is the emulation of the Bose-Hubbard model using ⁸⁷Rb atoms; this has led to detailed theoretical and experimental studies on both the superfluid-insulators transition and nonequilibrium quantum dynamics of this model [1,2,9–14]. Another such example is the emulation of the tilted Bose-Hubbard model, which has led to realization of translation symmetry-broken ground states in these systems [6,7,15–17].

More recently, experimental systems involving ultracold Rydberg atoms have been experimentally realized [18–21]. These atoms experience strong interatomic van der Waals interaction in their excited state leading to a Rydberg blockade with a tunable blockade radius [22,23]. An array of such atoms in a one-dimensional (1D) optical lattice, namely a Rydberg chain, is known to host both Ising and non-Ising quantum critical points [24,25]; the signature of the associated phase transition has been experimentally verified [20]. The nonequilibrium dynamics of such atoms has also been theoretically studied [26–33]. Interestingly, the violation of the eigenstate thermalization hypothesis (ETH) [34,35] for dynamics starting from a class of initial states has been experimentally observed in these systems [21]; this phenomenon has been explained by invoking the existence of an atypical set of athermal midspectrum quantum states, namely quantum scars [28–31]. The presence of such scars in the eigenspectrum of the Floquet Hamiltonian of a periodically driven Rydberg chain has also been predicted [32,33].

A natural extension of the above-mentioned studies on Rydberg chains is to investigate higher-dimensional Rydberg atom arrays. Such arrays are expected to host a rich variety of quantum ground states that have no 1D analogs. For the 2D square arrays, such studies have predicted the presence of several translational symmetry-broken ground states with definite density-wave orders; these ordered states are separated from the featureless disordered ground state via a second-order phase transition [36,37]. In more complicated nonbipartite lattices such as the kagome lattice, where the atoms are designed to occupy the links of the lattice (or equivalently sites of a ruby lattice), such atom arrays are predicted to host a spin-liquid quantum ground state over a wide parameter regime [38]. More recently, phases of Rydberg atoms on a 3D pyrochlore lattice have also been studied [39]. However, the nonequilibrium dynamics of such atom arrays has not been studied so far.

In this work, we shall study the prethermal Floquet phases of a periodically driven Rydberg atom array arranged as a rectangular lattice. The effective Hamiltonian of such an array can be described in terms of two states on a site with coordinate $\vec{r} = (j_x, j_y)$. The first of these is the ground state of the atoms; we shall denote this by $|g_{\vec{r}}\rangle$. The other state is the Rydberg excited state and is denoted by $|e_{\vec{r}}\rangle$. Using these as the basis states at each site, we can write the effective Hamiltonian of these atoms as [18–21]

$$H = \sum_{\vec{r}} \left(\Omega \sigma_{\vec{r}}^x - \frac{\Delta}{2} \sigma_{\vec{r}}^z \right) + \frac{1}{2} \sum_{\vec{r}, \vec{r}'} V(|\vec{r} - \vec{r}'|) \hat{n}_{\vec{r}} \hat{n}_{\vec{r}'}, \quad (1)$$

where $\sigma_{\vec{r}}^x$ are Pauli matrices in the space of states described above, $\sigma_{\vec{r}}^x = |g_{\vec{r}}\rangle\langle e_{\vec{r}}| + |e_{\vec{r}}\rangle\langle g_{\vec{r}}|$, and $\hat{n}_{\vec{r}} = (1 + \sigma_{\vec{r}}^z)/2$ is the Rydberg excitation density at the site \vec{r} of the lattice. Here $\Omega > 0$ denotes the coupling strength between the ground state and the Rydberg excited state, Δ denotes the detuning, which we shall assume to be uniform throughout the array, and $V(|\vec{r} - \vec{r}'|) = V_0/|\vec{r} - \vec{r}'|^6$ denotes the van der Waals

interaction between two Rydberg excitations with strength V_0 . In what follows, we shall drive the detuning parameter, Δ , of the model periodically with drive amplitude Δ_0 and frequency $\omega_D = 2\pi/T$, where T is the time period. For the square-pulse protocol, the drive term is given by

$$\begin{aligned} \Delta(t) &= \delta - \Delta_0 \text{ for } 0 \leq t < T/2 \\ &= \delta + \Delta_0 \text{ for } T/2 \leq t < T, \end{aligned} \quad (2)$$

and $\Delta(t+T) = \Delta(t)$, while for the cosine drive protocol, we have

$$\Delta(t) = \delta + \Delta_0 \cos(\omega_D t). \quad (3)$$

In this work, we shall restrict ourselves to the regime where the drive amplitude is large: $\Delta_0 \gg \delta, \Omega, V_0$.

The main results that we obtain in this work are as follows. First, using Floquet perturbation theory (FPT), which uses the inverse drive amplitude as the small parameter [40–43], we obtain an analytic, albeit perturbative, Floquet Hamiltonian for the driven system for both the square-pulse [Eq. (2)] and the cosine [Eq. (3)] protocols. Our analysis reveals several ordered Floquet phases with distinct density-wave orders, which are separated from the disordered state by second-order critical points. We also show that tuning the drive frequency allows us to tune the system between these phases and through the critical points. Second, we complement our results obtained from the analytical Floquet Hamiltonian with that from numerical exact diagonalization (ED) starting from H [Eq. (1)] with $\Delta(t)$ given by Eq. (2). Our study reveals the existence of an exponentially long prethermal timescale in the large and intermediate drive amplitude regime; the properties of the driven system up to this timescale are well described by the analytic Floquet Hamiltonian. Third, using the exact evolution operator obtained from ED, we compute the density-density correlation function of Rydberg excitations of the driven atom array after n cycles of the drive. We show that such a correlator exhibits qualitatively distinct behavior in the density-wave ordered and disordered Floquet phases; thus it serves as an experimentally relevant marker for the Floquet phases and the transitions between them. We demonstrate this explicitly for the disordered to the star and the checkerboard ordered Floquet phases (see Fig. 1); we find that the above-mentioned correlation function displays distinct long-time behaviors in the ordered and disordered phases as well as at the transition point between them. Thus it can be used to distinguish between these Floquet phases and also locate the transition between them. Finally, we discuss experiments that can test our theory, and possible extensions of our study in these systems.

The plan of the rest of the paper is as follows. In Sec. II, we derive the analytic Floquet Hamiltonian using FPT. This is followed by Sec. III, where we compare its prediction to numerical results obtained using ED, and we obtain the phase diagram of the driven system. Next, in Sec. IV, we compute the correlation function C , study its behavior in different Floquet phases, and also discuss the stability of these phases. Finally, we chart out experiments that can verify our theory, discuss possible extensions of it in these systems, and conclude in Sec. V.

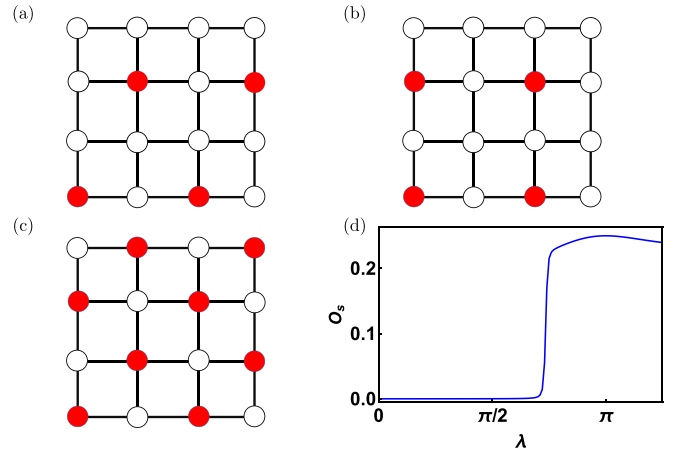


FIG. 1. Schematic representations of the (a) star, (b) striated, and (c) checkerboard phases. The red circles indicate sites with Rydberg excitations, while the white ones represent atoms in their ground state. (d) Plot of O_s obtained using exact eigenstates of $U(T, 0)$ as a function $\lambda = \Delta_0 T / (4\hbar)$, where T is the time period of a square pulse [Eq. (2)] for $V_0 = 25\Omega$. The other parameters are $\delta = 2\Omega$, $\Delta_0 = 100\Omega$, $L_x = 6$, and $L_y = 4$.

II. ANALYTIC FLOQUET HAMILTONIAN

In this section, we shall derive the analytic Floquet Hamiltonian for both the cosine and the square-pulse protocols using FPT. The details of the FPT method can be found in Refs. [40–43].

To obtain the Floquet Hamiltonian, we first rewrite $H(t) = H_0(t) + H_1$, where

$$\begin{aligned} H_0(t) &= -\frac{\Delta(t) - \delta}{2} \sum_{\vec{r}} \sigma_{\vec{r}}^z, \\ H_1 &= H_{1a} + H_{1b}, \quad H_{1a} = \sum_{\vec{r}} \Omega \sigma_{\vec{r}}^x, \\ H_{1b} &= -\sum_{\vec{r}} \frac{\delta}{2} \sigma_{\vec{r}}^z + \frac{1}{2} \sum_{\vec{r}, \vec{r}'} V(|\vec{r} - \vec{r}'|) \hat{n}_{\vec{r}} \hat{n}_{\vec{r}'}. \end{aligned} \quad (4)$$

This decomposition of $H(t)$ is made such that the term with the largest amplitude, Δ_0 , is included in H_0 . We have also separated the terms in H_1 into those that commute (H_{1b}) with H_0 and those that do not (H_{1a}).

Next, we construct the evolution operator $U_0(t, 0) = \mathcal{T}_t \exp[-i \int_0^t H_0(t') dt' / \hbar]$ (where \mathcal{T}_t is the time-ordering operator) corresponding to $H_0(t)$. For the square-pulse protocol, this yields

$$\begin{aligned} U_s^{(0)}(t, 0) &= e^{-i\Delta_0 t \sum_{\vec{r}} \sigma_{\vec{r}}^z / 2\hbar} \text{ for } 0 \leq t < T/2, \\ &= e^{-i\Delta_0(T-t) \sum_{\vec{r}} \sigma_{\vec{r}}^z / 2\hbar} \text{ for } T/2 \leq t < T, \end{aligned} \quad (5)$$

while for the cosine protocol we obtain

$$U_c^{(0)}(t, 0) = e^{i\Delta_0 \sin(\omega_D t) \sum_{\vec{r}} \sigma_{\vec{r}}^z / (2\hbar\omega_D)}. \quad (6)$$

Note that for both protocols, $U_0(T, 0) = I$, where I denotes the identity matrix; hence the zeroth-order Floquet Hamiltonian is $H_F^{(0)} = 0$.

To find the first-order terms, we use standard perturbation theory, which yields [43]

$$U_{c(s)}^{(1)}(T, 0) = -\frac{i}{\hbar} \int_0^T dt U_{c(s)}^{(0)\dagger}(t, 0) H_1 U_{c(s)}^{(0)}(t, 0). \quad (7)$$

To evaluate $U_{c(s)}^{(1)}$, we first note that the terms in H_{1b} [Eq. (4)] that commute with $U_{c/s}^{(0)}$ can be evaluated simply. This yields

$$\begin{aligned} U_{c(s)}^{(1b)}(T, 0) &= -\frac{iT}{\hbar} H_{1b}, \\ H_{Fc(s)}^{(1b)} &= \frac{i\hbar}{T} U_{c(s)}^{(1b)}(T, 0) = H_{1b}. \end{aligned} \quad (8)$$

To evaluate the contribution of H_{1a} to $U_{c(s)}^{(1)}$, we first note that $U_{c(s)}^{(0)}$ is diagonal in the Fock basis and can be written as

$$\begin{aligned} U_s^{(0)}(t, 0) &= e^{-i\Delta_0 t E_m / (2\hbar)} |m\rangle\langle m| \quad t \leq T/2 \\ &= e^{-i\Delta_0 (T-t) E_m / (2\hbar)} |m\rangle\langle m| \quad t > T/2, \\ U_c^{(0)}(t, 0) &= e^{i\Delta_0 E_m \sin \omega_D t / (2\hbar \omega_D)} |m\rangle\langle m|, \end{aligned} \quad (9)$$

where $|m\rangle$ denotes a Fock state with m Rydberg excitations (or equivalently m spin-up sites) and $L^2 - m$ atoms in their ground state, and E_m is the eigenvalue of $\sum_{\vec{r}} \sigma_{\vec{r}}^z$ in the state $|m\rangle$. We note that these states are degenerate since their energies do not depend on the positions of the Rydberg excitations. In this picture, it is easy to see that H_{1a} changes the number of such Rydberg excitations in any state by ± 1 ; thus $H_{1a}|m\rangle \sim |m+1\rangle + |m-1\rangle$. Furthermore, the energy differences between the states $|m\rangle$ and $|m \pm 1\rangle$ are given by $\Delta E_m^\pm = E_m - E_{m \pm 1} = \mp 2$. Using this, and after some standard algebra detailed in Ref. [33], we find

$$\begin{aligned} H_{Fc}^{(1a)} &= \Omega J_0 \left(\frac{2\lambda}{\pi} \right) \sum_{\vec{r}} \sigma_{\vec{r}}^x, \\ H_{Fs}^{(1a)} &= \Omega \frac{\sin \lambda}{\lambda} \sum_{\vec{r}} (\cos \lambda \sigma_{\vec{r}}^x - \sin \lambda \sigma_{\vec{r}}^y), \end{aligned} \quad (10)$$

where $\lambda = \Delta_0 T / (4\hbar)$, and J_0 denotes the zeroth-order Bessel function. The final first-order Floquet Hamiltonian is given by

$$H_{Fc(s)}^{(1)} = H_{Fc(s)}^{(1a)} + H_{Fc(s)}^{(1b)}. \quad (11)$$

The expressions of $H_F^{(1)}$ for both protocols suggest the existence of special drive frequencies at which, for a given drive amplitude Δ_0 , $H_F^{(1a)}$ vanishes. The frequencies correspond to $\lambda = m\pi$, where m is a nonzero integer, for the square-pulse protocol and $\lambda = \pi \eta_m / 2$ for the cosine protocol, where η_m denotes the value of the m th zero of J_0 . They are given by

$$\begin{aligned} \omega_m^* &= \frac{\Delta_0}{2m\hbar} \text{ for the square-pulse protocol} \\ &= \frac{\Delta_0}{\eta_m \hbar} \text{ for the cosine protocol.} \end{aligned} \quad (12)$$

At these frequencies, $[H_F^{(1)}, \hat{n}_{\vec{r}}] = 0$ leading to an approximate emergent conservation of $\hat{n}_{\vec{r}}$. This conservation is approximate since it is not respected by higher-order terms in the Floquet Hamiltonian.

To qualitatively understand the phases of $H_F^{(1)}$, we now consider the regime where $V_0, \delta \ll \Delta_0$. In this regime for

$\omega_D \gg \omega_1^*$, the ground state of $H_F^{(1)}$ is expected to be similar to the disordered paramagnetic phase found in Ref. [36]. In contrast, at $\omega_D = \omega_1^*$, the ground state of $H_F^{(1)}$ constitutes a density-wave ordered state whose precise nature depends on the relative strength of δ/Ω and V_0/Ω [36]. Thus as we tune the drive frequency towards ω_1^* , we expect to find a second-order phase transition between these phases. Also, in the regime of large Δ_0 , the higher-order corrections to $H_F^{(1)}$ are expected to be small; thus such phases should persist as long-lived prethermal phases of the driven system. We shall explore these phases in detail in Sec. III and their detection in Sec. IV A.

Before ending this section, we note that the effect of having $V_0 \gg \delta, \Omega$ is to preclude Rydberg excitations on the neighboring sites of the lattice. In this regime, it is possible to obtain a slightly modified form of the Floquet Hamiltonian which supports similar phases. Such a prohibition can be implemented by using a local projection operator

$$P_{\vec{r}} = (1 - \sigma_{\vec{r}}^z) / 2 \quad (13)$$

as shown in Ref. [18]. In this regime, the projected Hamiltonian is given by [18,24,25]

$$\begin{aligned} H_p(t) &= \sum_{\vec{r}} \left(\Omega \tilde{\sigma}_{\vec{r}}^x - \frac{\Delta(t)}{2} \sigma_{\vec{r}}^z \right) + \frac{1}{2} \sum'_{\vec{r}, \vec{r}'} V(|\vec{r} - \vec{r}'|) \hat{n}_{\vec{r}} \hat{n}_{\vec{r}'} \\ \tilde{\sigma}_{\vec{r}}^x &= P_{j_x-1, j_y} P_{j_x, j_y-1} \sigma_{j_x, j_y}^x P_{j_x+1, j_y} P_{j_x, j_y+1}, \end{aligned} \quad (14)$$

where \sum' denotes a sum over sites where \vec{r} is not a nearest neighbor of \vec{r}' . Note that $\tilde{\sigma}_{\vec{r}}^x$ can create a Rydberg excitation at site \vec{r} only if all its neighbors are in their ground states.

We can carry out an exactly similar perturbative analysis, charted out earlier in this section, starting from $H_p(t)$. The computation involved is almost identical to that used to obtain $H_F^{(1)}$, and we do not repeat it here. Such an analysis yields the Floquet Hamiltonians for the continuous and the square-pulse protocols for the projected case,

$$\begin{aligned} H_{Fc}^{p(1)} &= \Omega J_0 \left(\frac{2\lambda}{\pi} \right) \sum_{\vec{r}} \tilde{\sigma}_{\vec{r}}^x + \frac{1}{2} \sum'_{\vec{r}, \vec{r}'} V(|\vec{r} - \vec{r}'|) \hat{n}_{\vec{r}} \hat{n}_{\vec{r}'} \\ &\quad - \frac{\delta}{2} \sum_{\vec{r}} \sigma_{\vec{r}}^z, \\ H_{Fs}^{p(1)} &= \Omega \frac{\sin \lambda}{\lambda} \sum_{\vec{r}} (\cos \lambda \tilde{\sigma}_{\vec{r}}^x - \sin \lambda \tilde{\sigma}_{\vec{r}}^y) \\ &\quad + \frac{1}{2} \sum'_{\vec{r}, \vec{r}'} V(|\vec{r} - \vec{r}'|) \hat{n}_{\vec{r}} \hat{n}_{\vec{r}'} - \frac{\delta}{2} \sum_{\vec{r}} \sigma_{\vec{r}}^z. \end{aligned} \quad (15)$$

We note that the phases of $H_F^{p(1)}$ are qualitatively similar to those of $H_F^{(1)}$; in particular, we can still tune the drive frequency towards ω_1^* to obtain density-wave phases. The numerical advantage provided by $H_F^{p(1)}$ comes from the fact that the dimension of its Hilbert space, $\mathcal{D}_p \sim 1.503^{L^2}$ [44], grows slowly with system size L^2 compared to its counterpart \mathcal{D} for $H_F^{(1)}$, $\mathcal{D} \sim 2^{L^2}$. We shall use this fact while dealing with numerical analysis of the Floquet phases in subsequent sections.

III. PRETHERMAL FLOQUET PHASES

In this section, we study the Floquet phases using both the analytically obtained Floquet Hamiltonian [Eq. (15)] and the Floquet eigenstates obtained from exact numerical diagonalization of $U(T, 0)$. The numerical results presented in this section will be obtained for the square-pulse protocol with large V_0 . We shall also use the constraint that two neighboring sites cannot be simultaneously occupied by Rydberg excitations: $\hat{n}_{\mathbf{r}}\hat{n}_{\mathbf{r}'} = 0$ if \mathbf{r} and \mathbf{r}' are nearest neighbors. This approximation, which becomes accurate at large V_0 , allows us to access larger system size; the validity of this approximation will be discussed in detail in Sec. V.

For the square-pulse protocol and within the constrained subspace mentioned above, we can write the evolution operator as $U(T, 0) = U_+(T, T/2)U_-(T/2, 0)$, where

$$\begin{aligned} U_-(t, 0) &= \exp[-iH_p(\Delta_-)t/\hbar], \\ U_+(t, T/2) &= \exp[-iH_p[\Delta_+](t - T/2)/\hbar], \end{aligned} \quad (16)$$

where $\Delta_{\pm} = \delta \pm \Delta_0$ [Eq. (2)].

To obtain the exact Floquet eigenstates, we first numerically diagonalize $H_{p\pm} \equiv H_p(\Delta_{\pm})$. This allows us to obtain its eigenvalues and corresponding eigenvectors: $H_{p\pm}|q_{\pm}\rangle = E_{q_{\pm}}|q_{\pm}\rangle$. Using these, we can write the evolution operator as

$$\begin{aligned} U(T, 0) &= \sum_{q_+, q_+'} \mathcal{U}_{q_+, q_+'} |q_+\rangle \langle q_+'|, \\ \mathcal{U}_{q_+, q_+'} &= \sum_{p_-} e^{i(E_{q_+} + E_{p_-})T/(2\hbar)} c_{q_+, p_-}^* c_{q_+, p_-}, \end{aligned} \quad (17)$$

where $c_{\alpha\beta} = \langle \beta | \alpha \rangle$ are the overlap coefficients between eigenstates of H_+ and H_- . Using the matrix elements $\mathcal{U}_{q_+, q_+'}$ [Eq. (17)], we can numerically diagonalize $U(T, 0)$ to obtain its eigenvalues and eigenfunctions,

$$U(T, 0)|m\rangle = \Lambda_m(T)|m\rangle, \quad \Lambda_m(T) = e^{i\theta_m(T)}, \quad (18)$$

where the form of the eigenvalues Λ_m follows from the unitary nature of the evolution operator. We note that the $|m\rangle$'s are also eigenstates of the exact Floquet Hamiltonian H_F within the constrained subspace; their eigenvalues which correspond to the Floquet quasienergies are given by

$$\epsilon_m = \arccos[\text{Re}\Lambda_m(T)]\hbar/T. \quad (19)$$

In the limit of high drive frequency where T is sufficiently small, all the eigenvalues fall within the first Floquet Brillouin zone: $-\pi\hbar/T \leq \epsilon_m \leq \pi\hbar/T$. In this case, one can meaningfully order the quasienergies ϵ_m ; the lowest ϵ_m corresponds to the Floquet ground state and characterizes the Floquet phase. For lower drive frequencies, the quasienergies are no longer restricted within the first Floquet Brillouin zone; in this regime, they can be folded back using the standard reduced zone scheme [43]. However, this makes it impossible to order them by their magnitude. In this section, we shall work in the high drive frequency regime where the eigenvalues can be ordered.

To characterize the properties of these eigenvalues, we now define the order parameters corresponding to various ordered phases of this model [36,37]. These ordered states, namely the star, the striated, and the checkerboard states, are schematically sketched in Figs. 1(a), 1(b) and 1(c), respectively. To

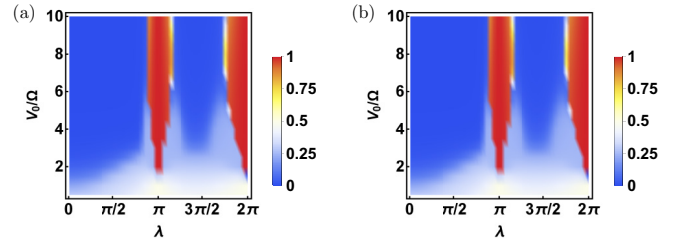


FIG. 2. (a) Plot of O_0 obtained using eigenstates of $H_{F_s}^{p(1)}$ as a function of V_0 and $\lambda = \Delta_0 T/(4\hbar)$, where T is the time period of a square pulse [Eq. (2)]. The dark red region corresponds to the star order for which $O_0 \simeq 1$, the white region corresponds to the checkerboard order for which $O_0 \simeq 1/2$, and the light blue region denotes the striated order for which $O_0 \simeq 1/4$. The dark blue region represents a disordered phase for which $O_0 = 0$. For these plots, $\delta = 0.75\Omega$, $\Delta_0 = 100\Omega$, $L_x = 6$, and $L_y = 4$. (b) Same as (a) but obtained using exact numerical diagonalization of $U(T, 0)$ within the projected Hilbert space.

characterize such orders, we label the sites of an $L_x \times L_y$ lattice by an integer

$$j = (j_x - 1) + (j_y - 1)L_x, \quad (20)$$

where $1 \leq j_y \leq L_y$ is the row index of the array, and $1 \leq j_x \leq L_x$ is the x coordinate of the site. We then define an operator

$$\hat{O}_c = \frac{1}{L} \sum_j (-1)^{j+[j/L_x]} (\hat{n}_j - 1/2), \quad (21)$$

where $[x]$ denotes the largest integer smaller than or equal to x and $L = L_x L_y$. It is straightforward to see that $|\langle \hat{O}_c \rangle| = 1/2$ for the checkerboard phase, $1/4$ for the striated phase, and 0 for the star phase. In contrast, the operator \hat{O}_s , defined as

$$\hat{O}_s = \frac{1}{L} \sum_j (-1)^{j+[j/(2L_x)]} (\hat{n}_j - 1/2) \quad (22)$$

vanishes for the checkerboard and striated phase; for the star phase, $|\langle \hat{O}_s \rangle| = 1/4$. A representative plot showing behavior of O_s across the transition from the paramagnetic to the star phase is shown in Fig. 1(d); we find that such a plot indicates a transition around $\lambda \simeq 3\pi/4$ for $V_0 = 25\Omega$, $\delta = 2\Omega$, and $\Delta_0 = 100\Omega$. The behavior of O_c for the transition from disordered to checkerboard or disordered to striated phases is similar.

To study the Floquet phases, we define a quantity

$$O_0 = |\langle m_0 | \hat{O}_c | m_0 \rangle| + 4|\langle m_0 | \hat{O}_s | m_0 \rangle|, \quad (23)$$

where $|m_0\rangle$ is the eigenstate corresponding to the lowest ϵ_m . This quantity allows us to distinguish between all three phases: $O_0 = 1/2$ ($1/4$) for the checkerboard (striated) phase and 1 for the star phase. In addition, both \hat{O}_c and \hat{O}_s vanish in the paramagnetic phase leading to $O_0 = 0$. We note here that O_0 cannot distinguish between partially ordered phases; however, such phases do not occur in the parameter regime of our study.

The left panel of Fig. 2 shows the plot of O_0 obtained using $H_{F_s}^{p(1)}$ [Eq. (15)] as a function of V_0/Ω and $\lambda = \Delta_0 T/(4\hbar)$ in the large drive amplitude regime ($\Delta_0 = 100\Omega$). The right panel of Fig. 2 shows a similar plot obtained using exact diagonalization of $U(T, 0)$ as discussed earlier in this section;

we find the two plots to be qualitatively similar for all V_0/δ when $V_0, \delta \ll \Delta_0$. This demonstrates the validity of the FPT in this regime.

In the high drive frequency regime where $\lambda \ll 1$, the plot reflects the presence of the paramagnetic phase (dark blue region) for which $O_0 = 0$ for $V_0 \gg \delta = 0.75\Omega$. In contrast, for $V_0 \sim \delta$, we find a smooth interpolation between the disordered and the checkerboard phase (light blue region). Such an interpolation is an artifact of using the constrained Hilbert space in our numerics; understandably, this approximation holds only for $V_0 \gg \delta$. The presence of the disordered phase at $V_0 \gg \delta$ and $\lambda \ll 1$ is consistent with the result of the first-order Magnus expansion for which the Floquet Hamiltonian is just the time-averaged value of $H(t)$ and is given by Eq. (1) with $\Delta \rightarrow \delta$. This model is known to have a paramagnetic phase for $V_0 \gg \delta$ in this regime [36].

For $V_0 \gg \delta$, we also find clear second-order transitions from the paramagnetic to the star phase as the drive time period T is varied. This transition occurs around $\lambda \simeq \pi, 2\pi$, where $\Omega_{\text{eff}} = \Omega \sin \lambda / \lambda \ll \delta, V_0$ [Eq. (12)]. For drive frequencies corresponding to $\lambda \simeq \pi, 2\pi$ and $V_0 \sim \delta$, we find the checkerboard phase (white region). By increasing V_0 and keeping $\lambda \simeq n\pi$ where n is an integer, we find a transition from the checkerboard to the star phase. This transition is expected to be first order since it is a transition between two phases with distinct classical orders. The disordered phase is absent since $\Omega_{\text{eff}} \simeq 0$ for these drive frequencies.

For lower drive frequencies, where the Floquet quasienergies are no longer restricted within the lowest Floquet Brillouin zone, we cannot order the eigenvalues. We note, however, that such ordered states still exist at the special drive frequencies given by $\lambda = n\pi$ as eigenstates of the Floquet Hamiltonian up to a prethermal timescale. Furthermore, their presence leaves a detectable signature in the correlation function of the systems, as we shall discuss in the next section.

IV. DETECTION AND STABILITY OF THE FLOQUET PHASES

In this section, we shall first discuss the properties of the correlation functions with which we can detect the Floquet phases. This will be followed by a study of the stability of these Floquet phases and the extent of the prethermal regime as a function of the drive amplitude. Throughout this section, we shall work within the projected Hilbert space as discussed earlier.

A. Correlation functions

In this subsection, we show that the Floquet phases and the transitions from the disordered paramagnetic to the star Floquet phases can be detected via a study of correlation functions. A similar detection scheme, as we shall discuss, is expected to hold for transitions from the disordered to other ordered states. This is of primary importance since, unlike equilibrium ground states, these phases do not correspond to standard energy eigenstates of a many-body system,

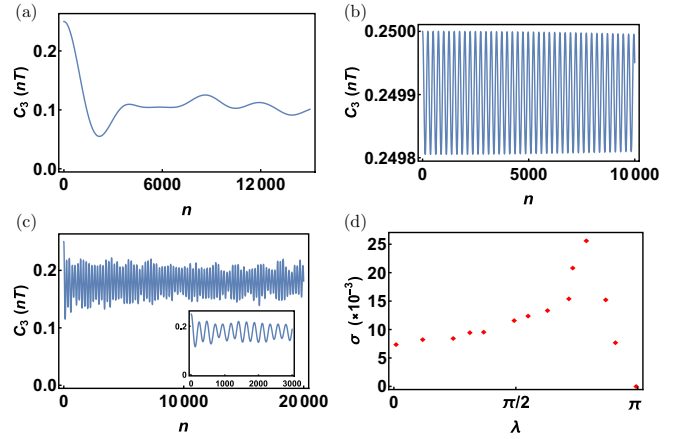


FIG. 3. Plot of $C_3(nT)$ across the transition from the disordered to the star phase. The plot shows $C_3(nT)$ as a function of the number of drive cycles n for (a) $\lambda = 0.05$, (b) π , and (c) 2.35. The inset in panel (c) reflects the long-time oscillations near the transition. The inset shows the details of this oscillating behavior on a shorter timescale. Panel (d) shows the fluctuation of the value of C_3 about its mean value as a function of λ . For all plots, $V_0 = 25\Omega$, $\delta = 2\Omega$, and $\Delta_0 = 100\Omega$. See the text for details.

and they cannot be accessed via standard thermodynamic measurements in experiments.

To this end, we compute the equal-time density-density correlation function of the driven system given by

$$C_3(nT) = \frac{1}{L} \sum_{\vec{r}\vec{a}} \langle \psi(nT) | \hat{n}_{\vec{r}} \hat{n}_{\vec{r}+\vec{a}} | \psi(nT) \rangle, \quad (24)$$

where \vec{a} is chosen so that \vec{r} and $\vec{r} + \vec{a}$ form third-nearest-neighboring sites of a 2D rectangular lattice. Note that the nearest-neighbor density-density correlation is identically zero within the projected Hilbert space, and the next-nearest-neighbor correlation is zero in the star phase and close to zero in the disordered phase; thus $C_3(nT)$ represents the most local correlation function with appreciable dynamical fluctuation.

The plot of $C_3(nT)$ is shown for three representative values of λ in Figs. 3(a), 3(b) and 3(c). In Fig. 3(a), $C_3(nT)$ is plotted as a function of n , the number of drive cycles, for $\lambda = 0.05$ and $V_0 = 25\Omega$ and starting from an initial Fock state $|\psi_0\rangle$ with star order (sketched in Fig. 1) so that $C_3(0) = 1/4$. The plot shows a rapid decay of the correlator towards its diagonal ensemble value ~ 0.1 , which is in accordance with the prediction of ETH. The oscillations around this value are a consequence of the finite system size. In contrast, for $\lambda = \pi$, as shown in Fig. 3(b), $C_3(nT)$ remains almost a constant showing very small oscillations around the initial value. This is a consequence of the fact that $|\psi_0\rangle$ is almost exactly an eigenstate of the exact Floquet Hamiltonian. We note that this will happen as long as $|\psi_0\rangle$ is a near-exact eigenstate of U or, equivalently, of H_F ; it need not necessarily be its lowest-lying eigenstate. In between, near the transition at $\lambda = 2.35$, we find that $C_3(nT)$ shows long-time oscillatory behavior which is distinct from its counterparts shown in Figs. 3(a) and 3(b). In particular, the oscillation amplitudes are larger than their counterparts in the ordered phase; also they are much longer-lived than

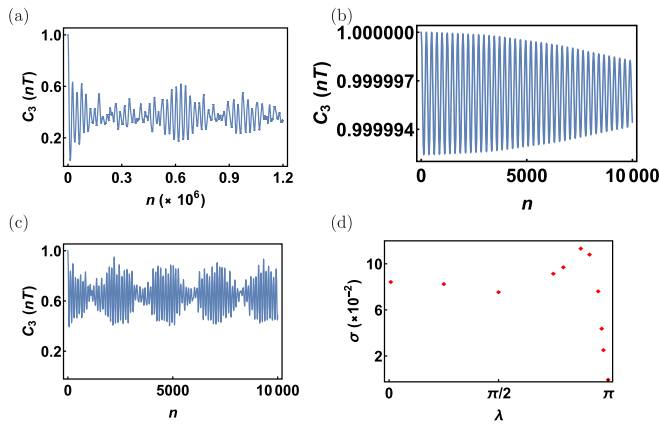


FIG. 4. Plot of $C_3(nT)$ across the transition from the disordered to the checkerboard phase. The plot shows $C_3(nT)$ as a function of the number of drive cycles n for (a) $\lambda = 0.025$, (b) π , and (c) 2.75. Panel (d) shows the fluctuation of $C_3(nT)$ about its mean value as a function of λ . For all plots, $V_0 = 1.5\Omega$, $\delta = \Omega$, and $\Delta_0 = 100\Omega$. See the text for details.

what is found in the disordered phase. This shows that $C_3(nT)$ can distinguish between the Floquet phases and provides a straightforward tool for their detection. The fluctuation of $C_3(nT)$ around its mean value at long-time is computed as

$$\sigma = \sqrt{\frac{1}{n_f - n_i} \sum_{n=n_i}^{n_f} C_3^2(nT) - \mu^2},$$

$$\mu = \frac{1}{n_f - n_i} \sum_{n=n_i}^{n_f} C_3(nT) \quad (25)$$

with $n_i = 3001$ and $n_f = 10000$.

A plot of σ as a function of λ is shown in Fig. 3(d). We find that σ indicates a clear peak at the transition point $\lambda = \lambda_c \simeq 2.3$ indicating a sharp increase in fluctuation of $C_3(nT)$ at the transition. It therefore serves as a distinguishing feature of the transition from a disordered to the star ordered phase.

A similar signature in the behavior of $C_3(nT)$ is also noticed when there is a transition between the checkerboard phase and the disordered phase at a lower value of the interaction potential V_0 . This is shown in Fig. 4 for $\delta = \Omega$ and $V_0 = 1.5\Omega$, where we choose a checkerboard ordered state as our initial state $|\psi_0\rangle$, so that $C_3(0) = 1$. Away from the transition [Figs. 4(a) and 4(b)], the fluctuation of $C_3(nT)$ is comparatively small, whereas close to the point of transition [Fig. 4(c)] it peaks considerably. In particular, when $\lambda = \pi$ in Fig. 4(c), the checkerboard state is almost an eigenstate of the exact evolution operator, which is why the quantum fluctuations dip to zero. In Fig. 4(d), we plot the average fluctuation of $C_3(nT)$, σ as a function of λ . The average is computed after the initial transient dynamics have settled down. It shows a peak around $\lambda = 2.75$. We later show in Fig. 6 that there is a phase transition from the disordered phase to the checkerboard phase precisely at this point even when the full Hilbert space is used instead of the projected subspace.

We note that such correlators are expected to show qualitatively similar behaviors across transitions from a disordered to any other ordered Floquet phase provided that we start from an initial Fock state which characterizes the order. However, it is not expected to provide a signature of a transition between two ordered phases; in this case, typically both of the ordered phases exist as eigenstates of the Floquet Hamiltonian across the transition, and the correlators do not evolve dynamically in either of the phases provided that the initial state is one of the ordered states.

Before ending this section, we would like to point out that the oscillations of $C_3(nT)$ found here are distinct from those expected due to the presence of quantum scars [27,32,45]. We have checked that such scars are absent in the spectrum of the Floquet Hamiltonian for $\delta \sim \Omega$; they are present, however, in the PXP limit ($\delta = 0$). A detailed study of the properties of such Floquet scars is left as the subject of future study.

B. Stability of the Floquet phases

In this section, we discuss the stability of such Floquet phases and provide an estimate of the prethermal timescale over which such phases are expected to exist. To this end, we first note that the behavior of a driven ergodic system is expected to be described by a local Floquet Hamiltonian only up to a finite, prethermal timescale t_p , where $\tau = t_p/T$. For $n > \tau$, the system is expected to heat up to infinite temperature and can no longer be described by a local Floquet Hamiltonian [46]. However, it is known, in the context of Magnus expansion, that $t_p \sim \exp[c\omega_D]$ (where c is a constant of order 1, which depends on the system details) in the high drive frequency limit [47]. It can thus be large leading to a long prethermal time over which the Floquet phases are expected to be stable.

To estimate the prethermal timescale τ for the driven Rydberg system, we plot $C_3(nT)$ as a function of the number of drive cycles n at $\lambda = \pi$ for several representative values of Δ_0/Ω . The value of $C_3(nT)$ obtained from $H_{Fs}^{p(1)}$ is a constant and equals 0.25 for $\lambda = \pi$; at large Δ_0 , such a constant value is also found for $C_3(nT)$ obtained using ED, as can be seen from Fig. 3(b). To characterize the difference between the results obtained using ED and that from $H_{Fs}^{p(1)}$, we therefore study the deviation of $C_3(nT)$ from its constant value.

The result of such a study is shown in Fig. 5. In Figs. 5(a), 5(b), and 5(c), we plot $C_3(nT)$, obtained using ED, as a function of n for $\lambda = \pi$. Figure 5(a) shows such a plot for a low drive amplitude $\Delta_0 = 0.9\Omega$; we find that $C_3(nT)$ deviates from its initial value within the first few drive cycles. The time taken to achieve this deviation increases with increasing Δ_0 [Fig. 5(b), where $\Delta_0 = 1.25\Omega$] and around $\Delta_0 = 1.45\Omega$, $C_3(nT)$ remains fixed at its constant value predicted by $H_{Fs}^{p(1)}$ for $n \gg 1500$ drive cycles.

From these plots, we can obtain a qualitative estimate of τ . Here we choose τ to be the smallest number of drive cycles at which $C_3(nT) \simeq 0.2$. The choice of $C_3(nT) \simeq 0.2$ as the cutoff is motivated by the fact that the infinite-temperature ensemble average of this correlator is close to 0.17. A plot of τ as a function of Δ_0 with $\lambda = \pi$ is shown in Fig. 5(d).

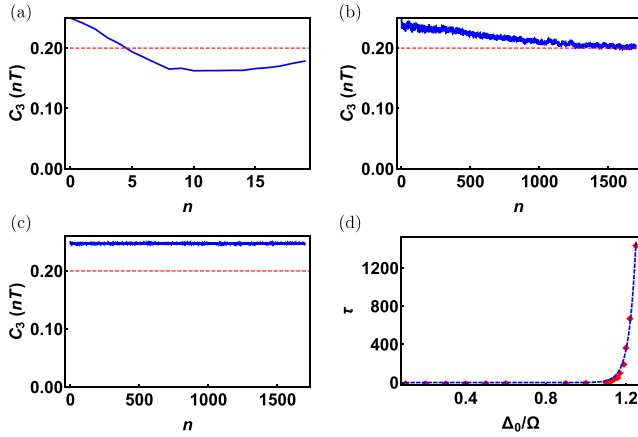


FIG. 5. Plot of $C_3(nT)$ as a function of n at $\lambda = \pi$ for (a) $\Delta_0/\Omega = 0.9$, (b) 1.25, and (c) 1.45. (d) Plot of τ , measured as the minimal number of cycles after which $C_3 \simeq 0.2$, as a function of Δ_0 showing an exponential growth of τ at large Δ_0 . For all plots, $V_0 = 25\Omega$ and $\delta = 2\Omega$. The red dotted lines in panels (a), (b), and (c) indicate the line $C_3 = 0.2$. See the text for details.

We find that τ shows a steep rise around $\Delta_0 \simeq \Omega, \delta$. This allows us to conclude that the Floquet phases are stable for a very long timescale as long as we are in the regime $\Delta_0 \gg \Omega, \delta$.

V. DISCUSSION

In this work, we have identified the Floquet phases of a periodically driven Rydberg atom array. Such phases can be tuned as a function of the drive frequency; our analysis identifies special drive frequencies that satisfy $\Delta_0 T/\hbar = 4m\pi$, where m is a positive integer, for a square-pulse protocol and $\Delta_0 T/\hbar = 2\pi\eta_m$ for a cosine protocol. At these drive frequencies, one finds density-wave ordered Floquet phases. In the high drive amplitude regime, we find a large prethermal timescale for which these Floquet phases are stable and are accurately derived by the analytical first-order Floquet Hamiltonian $H_F^{(1)}$ derived in Sec. II. We note here that although we have carried out all the numerics using the square-pulse protocol, the results of Sec. II strongly suggest that an analogous phenomenon exists for continuous drive protocols; the expression for the special frequencies for the cosine protocol is given by Eq. (12). We have also presented a method to detect these Floquet phases and the transitions between them via measurement of the equal-time density-density correlation function $C_3(nT)$. We note that the Floquet phases, unlike their thermodynamic counterparts, are not readily accessible in experiments; our results, therefore, provide a useful experimental tool for detection of these phases.

In the previous sections, we have used the approximation of large V_0 for obtaining these phases. This is not an essential feature of our analysis, as can be seen by comparing Eqs. (11) and (15). The first of these [Eq. (11)] obtains the Floquet Hamiltonian without any additional approximation for V_0 , while the second is derived in the large- V_0 regime. Both of these Floquet Hamiltonians provided identical expressions for the special frequencies ω_m^* [Eq. (12)]. The reason for choosing

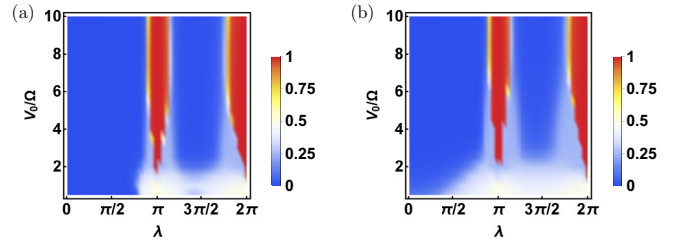


FIG. 6. Plot of O_0 as a function of V_0 and λ showing the Floquet phases obtained using ED starting from (a) $H_{F_S}^{(1)}$ [Eq. (11)] and keeping the full Hilbert space where neighboring Rydberg excitations are allowed, and (b) $H_p(t)$ [Eq. (14)] with the same square pulse protocol but working with the projected Hilbert space with no nearest-neighbor Rydberg excitations. For both plots, $\delta = 0.75\Omega$, $\Delta_0 = 100\Omega$, and $L_x = L_y = 4$.

the latter when it comes to exact numerics is that it has a smaller Hilbert space, which allows access to larger system sizes for carrying out ED. To ascertain this fact, we show a comparison in Fig. 6 between the Floquet phases obtained by applying ED on $H_{F_S}^{(1)}$ keeping the full Hilbert space and that obtained by diagonalizing U within the constrained Hilbert space. The result of the phase diagram obtained from $H_{F_S}^{(1)}$ is given in Fig. 6(a). Figure 6(b) shows the Floquet phases obtained using the projected subspace for $N = 16$ sites; the phase diagram is similar to the one obtained for $N = 24$ sites [Fig. 2(b)]. A comparison of this phase diagram with the one shown in Fig. 6(a) shows that they differ qualitatively only for $V_0 \leq \delta, \Omega$ and $\Delta_0 T/\hbar \ll \pi$; the spurious interpolating behavior obtained using the projected Hilbert space does not appear in this regime and is replaced by the disordered phase in the exact phase diagram. However, in other regimes, there is excellent agreement between the two phase diagrams including around $V_0 \simeq \delta$ when $\lambda \geq \pi$. The last feature owes its existence to the reduction of $\Omega_{\text{eff}} \sim \sin \lambda/\lambda$ in this regime, which is equivalent to an effective increase in V_0 .

Finally, we discuss experiments that can test our theory. We propose a standard experimental setup involving Rydberg atoms in a rectangular array where the detuning of these atoms is changed periodically with time according to either a square pulse or a cosine protocol. We predict the existence of special frequencies where the system should exhibit a star ordered Floquet phase at large V_0 . Such a phase would leave its imprint on the time evolution of the correlation function $C_3(nT)$ starting from an initial Fock state with star order; in the ordered phase, $C_3(nT)$ will be very nearly time-independent. The transition between the star and the disordered phase can be achieved by tuning the drive frequency; such a transition will be reflected in the behavior of $C_3(nT)$ as discussed in Sec. IV A. The preparation of the initial state for the study of the dynamics of $C_3(nT)$ can be achieved by standard techniques, which involves realization of such a state as the ground state of an undriven Rydberg Hamiltonian at a fixed large δ and V_0 followed by a sudden ramp of the optical lattice depth to freeze the desired Rydberg excitation configuration [18–20].

In conclusion, we have discussed the Floquet phases of Rydberg atoms arranged in a rectangular array. We have provided a way of experimentally detecting these phases and

the transitions between them via measurements of equal-time correlation functions; moreover, we have identified the high drive amplitude regime where such phases are stable over a long prethermal timescale. Within this timescale, their properties can be described by the first-order Floquet Hamiltonian obtained using FPT.

ACKNOWLEDGMENTS

S.G. acknowledges CSIR, India for support through Project No. 09/080(1133)/2019-EMR-I. D.S. thanks SERB, India for support through project JBR/2020/000043. K.S. thanks SERB, India for support through project JCB/2021/000030.

-
- [1] M. Greiner, O. Mandel, T. Esslinger, T. W. Hänsch, and I. Bloch, *Nature (London)* **415**, 39 (2002).
- [2] C. Orzel, A. K. Tuchman, M. L. Fenselau, M. Yasuda, and M. A. Kasevich, *Science* **291**, 2386 (2001).
- [3] I. Bloch, J. Dalibard, and W. Zwerger, *Rev. Mod. Phys.* **80**, 885 (2008).
- [4] T. Kinoshita, T. Wenger, and D. S. Weiss, *Nature (London)* **440**, 900 (2006).
- [5] L. E. Sadler, J. M. Higbie, S. R. Leslie, M. Vengalattore, and D. M. Stamper-Kurn, *Nature (London)* **443**, 312 (2006).
- [6] W. S. Bakr, A. Peng, M. E. Tai, R. Ma, J. Simon, J. I. Gillen, S. Folling, L. Pollet, and M. Greiner, *Science* **329**, 547 (2010).
- [7] H. Bernien, S. Schwartz, A. Keesling, H. Levine, A. Omran, H. Pichler, S. Choi, A. S. Zibrov, M. Endres, M. Greiner, V. Vuletic, and M. D. Lukin, *Nature (London)* **551**, 579 (2017).
- [8] See, for example, M. Lewenstein, A. Sanpera, and V. Ahufinger, *Ultracold Atoms in Optical Lattices: Simulating Quantum Many-body Systems* (Oxford University Press, Oxford, 2012).
- [9] M. P. A. Fisher, P. B. Weichman, G. Grinstein, and D. S. Fisher, *Phys. Rev. B* **40**, 546 (1989).
- [10] K. Sheshadri, H. R. Krishnamurthy, R. Pandit, and T. V. Ramakrishnan, *Europhys. Lett.* **22**, 257 (1993).
- [11] D. Jaksch, C. Bruder, J. I. Cirac, C. W. Gardiner, and P. Zoller, *Phys. Rev. Lett.* **81**, 3108 (1998).
- [12] J. K. Freericks and H. Monien, *Europhys. Lett.* **26**, 545 (1994); *Phys. Rev. B* **53**, 2691 (1996); W. Krauth and N. Trivedi, *Europhys. Lett.* **14**, 627 (1991); B. Capogrosso-Sansone, N. V. Prokof'ev, and B. V. Svistunov, *Phys. Rev. B* **75**, 134302 (2007).
- [13] K. Sengupta and N. Dupuis, *Phys. Rev. A* **71**, 033629 (2005); A. Rançon and N. Dupuis, *Phys. Rev. B* **83**, 172501 (2011); **84**, 174513 (2011).
- [14] C. Trefzger and K. Sengupta, *Phys. Rev. Lett.* **106**, 095702 (2011); J. K. Freericks, H. R. Krishnamurthy, Y. Kato, N. Kawashima, and N. Trivedi, *Phys. Rev. A* **79**, 053631 (2009).
- [15] S. Sachdev, K. Sengupta, and S. M. Girvin, *Phys. Rev. B* **66**, 075128 (2002); C. P. Rubbo, S. R. Manmana, B. M. Peden, M. J. Holland, and A. M. Rey, *Phys. Rev. A* **84**, 033638 (2011).
- [16] S. Pielawa, T. Kitagawa, E. Berg, and S. Sachdev, *Phys. Rev. B* **83**, 205135 (2011).
- [17] M. Kolodrubetz, D. Pekker, B. K. Clark, and K. Sengupta, *Phys. Rev. B* **85**, 100505(R) (2012).
- [18] S. Ebadi, T. T. Wang, H. Levine, A. Keesling, G. Semeghini, A. Omran, D. Bluvstein, R. Samajdar, H. Pichler, W. W. Ho, S. Choi, S. Sachdev, M. Greiner, V. Vuletic, and M. D. Lukin, *Nature (London)* **595**, 227 (2021).
- [19] D. Bluvstein, A. Omran, H. Levine, A. Keesling, G. Semeghini, S. Ebadi, T. T. Wang, A. A. Michailidis, N. Maskara, W. W. Ho, S. Choi, M. Serbyn, M. Greiner, V. Vuletic, and M. Lukin, *Science* **371**, 1355 (2021).
- [20] G. Semeghini, H. Levine, A. Keesling, S. Ebadi, T. T. Wang, D. Bluvstein, R. Verresen, H. Pichler, M. Kalinowski, R. Samajdar, A. Omran, S. Sachdev, A. Vishwanath, M. Greiner, V. Vuletic, and M. D. Lukin, *Science* **374**, 1242 (2021).
- [21] A. Gaëtan, Y. Miroshnychenko, T. Wilk, A. Chotia, M. Viteau, D. Comparat, P. Pillet, A. Browaeys, and P. Grangier, *Nat. Phys.* **5**, 115 (2009).
- [22] D. Tong, S. M. Farooqi, J. Stanojevic, S. Krishnan, Y. P. Zhang, R. Cote, E. E. Eyler, and P. L. Gould, *Phys. Rev. Lett.* **93**, 063001 (2004); M. D. Lukin, M. Fleischhauer, R. Cote, L. M. Duan, D. Jaksch, J. I. Cirac, and P. Zoller, *ibid.* **87**, 037901 (2001).
- [23] E. Urban, T. A. Johnson, T. Henage, L. Isenhower, D. D. Yavuz, T. G. Walker, and M. Saffman, *Nat. Phys.* **5**, 110 (2009).
- [24] R. Ghosh, A. Sen, and K. Sengupta, *Phys. Rev. B* **97**, 014309 (2018); R. Samajdar, S. Choi, H. Pichler, M. D. Lukin, and S. Sachdev, *Phys. Rev. A* **98**, 023614 (2018).
- [25] P. Fendley, K. Sengupta, and S. Sachdev, *Phys. Rev. B* **69**, 075106 (2004).
- [26] K. Sengupta, S. Powell, and S. Sachdev, *Phys. Rev. A* **69**, 053616 (2004).
- [27] B. Mukherjee, A. Sen, D. Sen, and K. Sengupta, *Phys. Rev. B* **102**, 014301 (2020).
- [28] C. J. Turner, A. A. Michailidis, D. A. Abanin, M. Serbyn, and Z. Papic, *Nat. Phys.* **14**, 745 (2018); *Phys. Rev. B* **98**, 155134 (2018).
- [29] K. Bull, I. Martin, and Z. Papic, *Phys. Rev. Lett.* **123**, 030601 (2019); S. Moudgalya, N. Regnault, and B. A. Bernevig, *Phys. Rev. B* **98**, 235156 (2018).
- [30] V. Khemani, C. R. Laumann, and A. Chandran, *Phys. Rev. B* **99**, 161101(R) (2019).
- [31] T. Iadecola, M. Schechter, and S. Xu, *Phys. Rev. B* **100**, 184312 (2019).
- [32] B. Mukherjee, S. Nandy, A. Sen, D. Sen, and K. Sengupta, *Phys. Rev. B* **101**, 245107 (2020).
- [33] B. Mukherjee, A. Sen, D. Sen, and K. Sengupta, *Phys. Rev. B* **102**, 075123 (2020).
- [34] For a review, see L. D'Alessio, Y. Kafri, A. Polkovnikov, and M. Rigol, *Adv. Phys.* **65**, 239 (2016); A. Polkovnikov, K. Sengupta, A. Silva, and M. Vengalattore, *Rev. Mod. Phys.* **83**, 863 (2011).
- [35] J. M. Deutsch, *Phys. Rev. A* **43**, 2046 (1991); M. Srednicki, *Phys. Rev. E* **50**, 888 (1994); *J. Phys. A* **32**, 1163 (1999); M. Rigol, V. Dunjko, and M. Olshanii, *Nature (London)* **452**, 854 (2008).
- [36] R. Samajdar, W. W. Ho, H. Pichler, M. D. Lukin, and S. Sachdev, *Proc. Natl. Acad. Sci. (USA)* **118**, e2015785118 (2021); M. Kalinowski, R. Samajdar, R. G. Melko, M. D. Lukin, S. Sachdev, and S. Choi, *Phys. Rev. B* **105**, 174417 (2022).

- [37] Z. Yan, R. Samajdar, Y.-C. Wang, S. Sachdev, and Z. Y. Meng, *Nat. Commun.* **13**, 5799 (2022); R. Samajdar, D. G. Joshi, Y. Teng, and S. Sachdev, *Phys. Rev. Lett.* **130**, 043601 (2023).
- [38] R. Verresen, M. D. Lukin, and A. Vishwanath, *Phys. Rev. X* **11**, 031005 (2021).
- [39] J. Shah, G. Nambiar, A. V. Gorshkov, and V. Galitski, [arXiv:2301.04657](https://arxiv.org/abs/2301.04657).
- [40] A. Soori and D. Sen, *Phys. Rev. B* **82**, 115432 (2010).
- [41] T. Bilitewski and N. R. Cooper, *Phys. Rev. A* **91**, 063611 (2015).
- [42] A. Haldar, D. Sen, R. Moessner, and A. Das, *Phys. Rev. X* **11**, 021008 (2021).
- [43] A. Sen, D. Sen, and K. Sengupta, *J. Phys.: Condens. Matter* **33**, 443003 (2021).
- [44] R. J. Baxter, *Ann. Comb.* **3**, 191 (1999).
- [45] C. J. Lin, V. Calvera, and T. H. Hsieh, *Phys. Rev. B* **101**, 220304(R) (2020).
- [46] L. D'Alessio and M. Rigol, *Phys. Rev. X* **4**, 041048 (2014).
- [47] T. Kuwahara, T. Mori, and K. Saito, *Ann. Phys.* **367**, 96 (2016).